frontiers in Marine Science

TYPE Original Research
PUBLISHED 28 May 2026
DOI 10.3389/fmars.2026.1800486

Check for updates

OPEN ACCESS

EDITED BY
Yijun Xiong,
University of Leeds, United Kingdom

REVIEWED BY
Qiang Liu,
Ministry of Natural Resources, China
Debbrota Mallick,
University of Georgia, United States

*CORRESPONDENCE
Hepin Wu
hepinwu@njnu.edu.cn
Da Li
lida@nju.edu.cn

RECEIVED 31 January 2026
REVISED 20 April 2026
ACCEPTED 28 April 2026
PUBLISHED 28 May 2026

CITATION
Zhang Z, Wu H, Li Q, Tang X, Zhou H and Li D (2026) Biogeochemical evolution and iron speciation in the abandoned Yellow River Delta: deciphering the impact of anthropogenic engineering and introduced *Spartina alterniflora*. *Front. Mar. Sci.* 13:1800486. doi: 10.3389/fmars.2026.1800486

COPYRIGHT
© 2026 Zhang, Wu, Li, Tang, Zhou and Li. This is an open-access article distributed under the terms of the Creative Commons Attribution License (CC BY). The use, distribution or reproduction in other forums is permitted, provided the original author(s) and the copyright owner(s) are credited and that the original publication in this journal is cited, in accordance with accepted academic practice. No use, distribution or reproduction is permitted which does not comply with these terms.

Biogeochemical evolution and iron speciation in the abandoned Yellow River Delta: deciphering the impact of anthropogenic engineering and introduced *Spartina alterniflora*

Zisheng Zhang, Hepin Wu*, Qiao Li, Xiao Tang, Hongwu Zhou and Da Li*

Jiangsu Key Laboratory of Ocean-Land Environmental Change and Ecological Construction, School of Marine Science and Engineering, Nanjing Normal University, Nanjing, China

Understanding sediment dynamics and anthropogenic impacts in the land-sea interaction zone of the Abandoned Yellow River Delta is challenged by complex material sources. This study aims to reconstruct sedimentary environment evolution and evaluate human influences on silty-mud tidal flats. Sediment cores were collected from a bare flat (GT) and a *Spartina alterniflora* marsh (HM) in the Yancheng coastal wetland, Jiangsu, China. A multi-proxy approach was applied, including grain size, organic carbon and nitrogen content, ^{210}Pb - ^{137}Cs dating, analysis of major elements and iron speciation analysis. Results indicate: (1) The GT core exhibits sandy silt characteristics, indicative of an intertidal environment. The HM core is dominated by clayey silt and silt, displaying a silt-sand binary structure, reflecting a typical silty tidal flat. Grain size characteristics suggest tidal flat accretion is collectively driven by reclamation, storm surges, tidal action, and sediment trapping by *S. alterniflora*. (2) Organic matter provenance analysis reveals marine sources dominate the GT core, while terrigenous sources dominate the HM core. Increasing trends of TOC, TN, and C/N with depth suggest *S. alterniflora* introduction likely promoted organic matter accumulation. (3) ^{210}Pb - ^{137}Cs dating yields deposition rates of 1.25 cm/a (GT) and 1.39 cm/a (HM). Combined with previous studies, regional average deposition rates show a declining trend with enhanced accretion, potentially linked to increased hydrodynamics from reclamation and the Jiangsu Coastal Current. (4) Major elements follow the Na > Al > K > Fe > Ca > Ti > Mg > Ba > Mn > Sr and the distribution of major elements is synergistically controlled by provenance, grain size effects, and biological processes; the variations in element-grain size correlations reveal the modulating effect of sedimentary composition on geochemical behavior. (5) Iron speciation

content follows the order Fe_{ox} > Fe_{mag} > Fe_{carb} > Fe_{py} and increases with depth, primarily sourced from terrigenous inputs influenced by chemical weathering and marine dynamics. The sedimentary environment is oxic/suboxic, promoting TOC mineralization and hindering preservation. The Fe_{HR}/Fe_T ratio characteristics resemble those of shelf-margin marine sediments and Yellow River particulates. However, influenced by weathering, runoff, and sea-level changes, this ratio is unreliable for accurately indicating redox conditions.

KEYWORDS

anthropogenic impacts, iron speciation, sedimentary environment evolution, Subei Abandoned Yellow River Delta, tidal flat sediments

1 Introduction

The Abandoned Yellow River Delta of China is a geomorphological legacy formed during the period when the Yellow River captured the Huaihe River to discharge into the sea. Between 1128 and 1855, the Yellow River followed a southward course into the Yellow Sea, shaping a vast deltaic plain along the northern Jiangsu coast. Following the northward return of the Yellow River in 1855, the cessation of primary terrestrial sediment supply caused the region to enter an 'abandonment' phase (Zhang and Chen, 2014). It is located within a typical land-sea interaction zone (Milliman et al., 1987; Alexander et al., 1991; Xue et al., 2004). Its sedimentary environment has long been shaped by multiple dynamic forces, including riverine discharge, tides, waves, coastal currents, and storm surges (Wang et al., 2017). In recent decades, anthropogenic interventions such as coastal reclamation (He et al., 2021), hydraulic infrastructure development, and the introduction of the invasive species *Spartina. Alterniflora which was intentionally introduced for coastal protection and sediment trapping* (Xie et al., 2020; Feng et al., 2024a) have further restructured the regional sedimentary dynamic processes and geomorphological evolutionary pathways in this region.

As a key geomorphic unit in this region, silty-mud tidal flats exhibit profound potential for port construction, land reclamation, and intertidal aquaculture (Gao, 2017). Domestic research on such tidal flats has progressed in several dimensions. Regarding sedimentary dynamics, Gao et al. (2005) established a micro-geomorphic classification system for tidal flats encompassing five types: bare flat, *S. alterniflora* zones, *S. alterniflora-Suaeda salsa* mixed zones, *Suaeda salsa* zones, and phragmites australis zone, by analyzing surface and core sediments via laser grain-size analysis. This work clarified the distinct sedimentary characteristics of each ecological zone (Gao et al., 2005). Regarding ecological function, Zhou et al. (2024) assessed blue carbon reservoirs in the Yellow River Delta and Yancheng coastal wetlands, revealing that despite low unit-area organic carbon density, the extensive spatial footprint of tidal flats accounts for over 75% of regional organic carbon stocks (Zhou et al., 2024). Concerning anthropogenic impacts, Zhang et al. (2022) developed a coupled benthic-microgeomorphology model, demonstrating that augmented upstream runoff accelerates sediment accretion, which in turn bolsters the erosional resilience of tidal ecosystems (Zhang et al., 2022). Additionally, remote sensing and GIS applications have unraveled the "southern accretion, northern erosion" pattern of the Yellow River estuary tidal flats and its non-linear correlation with tidal creek development (Su et al., 2018).

Internationally, Morton et al., employed multi-source remote sensing data to verify that storm surges can significantly reshape tidal flat morphology in the short term, identifying them as pivotal drivers of transient coastal evolution (Morton and Blackmore, 2001). Through hydrodynamic-sediment coupling simulations, Roberts et al., employing a coupled hydrodynamic-sediment numerical model, proposed that increased wave energy or tidal range gradients can promote a steepening of the tidal flat profile, whereas ample sediment supply triggers a negative feedback mechanism, driving the profile toward an equilibrium state (Roberts et al., 2000). John et al. further utilized coupled models to reveal nonlinear feedback mechanisms between the rate of relative sea-level rise and coastal dynamic responses. They highlighted that the sensitivity of open coasts to the coupled effects of tidal pumping and longshore sediment transport is a key factor controlling the divergent evolutionary pathways of intertidal morphologies (Nicholls and Cazenave, 2010).

Iron, as a key redox-sensitive element in marine sediments, plays a critical role in the global carbon cycle (Raiswell and Canfield, 2012). Iron oxides, characterized by high specific surface areas and potent adsorption capacities, can facilitate the burial and preservation of organic carbon by forming iron-organic carbon complexes (Hu et al., 2023). While reactive iron is widely recognized for its capacity to facilitate organic carbon preservation in stable marine sediments, a critical data gap exists regarding its early diagenetic behavior in such highly disturbed, oxic-to-suboxic silty-mud tidal flats. Therefore, we test the central hypothesis that under the prevailing oxic-to-suboxic conditions of these tidal flats, the high input of terrigenous reactive iron promotes the mineralization of organic carbon rather than its long-term preservation. Additionally, we postulate that the interpretative precision of standard iron speciation proxies is significantly confounded by regional hydrogeochemical processes, rendering them unreliable as standalone *in-situ* redox indicators." To address these gaps, this study investigates sediment cores from bare flats and *S. alterniflora* marshes within the Yancheng coastal wetland of Jiangsu Province, China. Utilizing a multi-proxy approach including grain size analysis, organic carbon and nitrogen content, geochronology, and iron speciation, it aims to reconstruct the sedimentary evolutionary sequence of this region over the past century (Zhao et al., 2021). This study intends to

clarify the superimposed impacts of natural processes and anthropogenic activities (Milliman et al., 1987) on sedimentary properties. Furthermore, it delves into the indicative roles of iron species geochemistry for sedimentary environments and organic carbon preservation potential. These findings are expected to provide a robust scientific basis for regional ecological management and coastal carbon cycle assessments.

2 Materials and methods

2.1 Regional setting

The study area is situated in the Yancheng coastal wetland of Jiangsu Province, China (Figure 1). Located within the core region of the Abandoned Yellow River Delta (33°20′-34°30′N, 120°10′-120°50′E), the area experiences a subtropical monsoon climate. It is characterized by a flat topography dominated by extensive silt-mud tidal flats. A distinct zonation pattern develops from land to sea, comprising a *Phragmites australis* zone, a *Spartina alterniflora* zone, bare flats, and a tidal creek network.

Sediment sources in this area are complex, resulting from the mixing of historical alluvial deposits from the Abandoned Yellow River, fine-grained materials from the modern Yellow River transported over long distances, and sediments carried by the Jiangsu Coastal Current. The tidal regime is regular semidiurnal, with an average tidal range of 2.5-3.5 m. Tidal current dynamics serve as the primary factor controlling sediment resuspension and alongshore transport. Furthermore, storm surge events, occurring on average 1–2 times per year, play a significant role in the short-term reshaping of tidal flat morphology. Following its introduction in the 1980s, *Spartina alterniflora* has rapidly expanded. Its well-developed root systems and above-ground structures have markedly enhanced sediment trapping, thereby profoundly influencing sediment accumulation processes.

2.2 Sampling and analysis methods

Between July and August 2022, two sediment cores were retrieved from the Spartina alterniflora marsh (HM: 120°61'E, 33°61'N) and an adjacent bare flat (GT: 120°62'E, 33°61'N) within the Yancheng coastal wetland (Figure 2), with lengths of 54 cm and 103 cm, respectively. The cores were collected using a PVC gravity corer with a diameter of 76 mm and were immediately sectioned at 1 cm intervals in the field, yielding a total of 157 sub-samples. All sediment samples were sealed in low-adsorption bags (specifically designed for trace metals and Fe species) and stored at -25 °C in the laboratory until analysis. Throughout the sample preparation and analytical phases, strict Quality Assurance and Quality Control protocols were implemented to prevent contamination and ensure high analytical precision. Details of the experimental instrumentation used in this study are summarized in Table 1.

Grain size analysis was performed at the School of Marine Science and Engineering, Nanjing Normal University. Measurements were conducted using a Mastersizer 2000 laser diffraction particle size analyzer (Malvern Instruments Ltd., UK) with a detection range of 0.01–10000 μm. The relative error for replicate measurements was less than 3%. Based on the results, grain size parameters, including mean

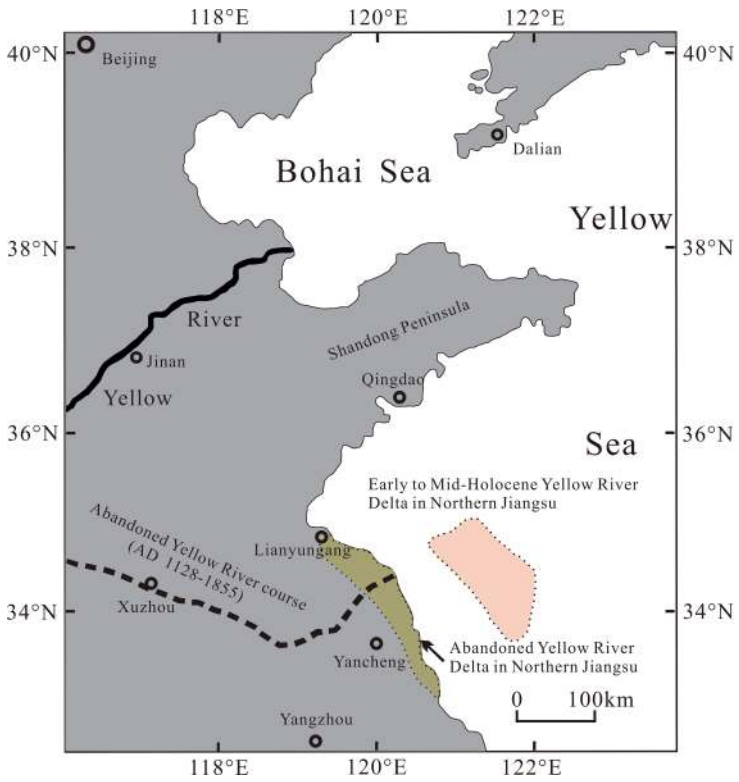


FIGURE 1
Regional map of the Abandoned Yellow River Delta. Modified from Xia et al. (2021).

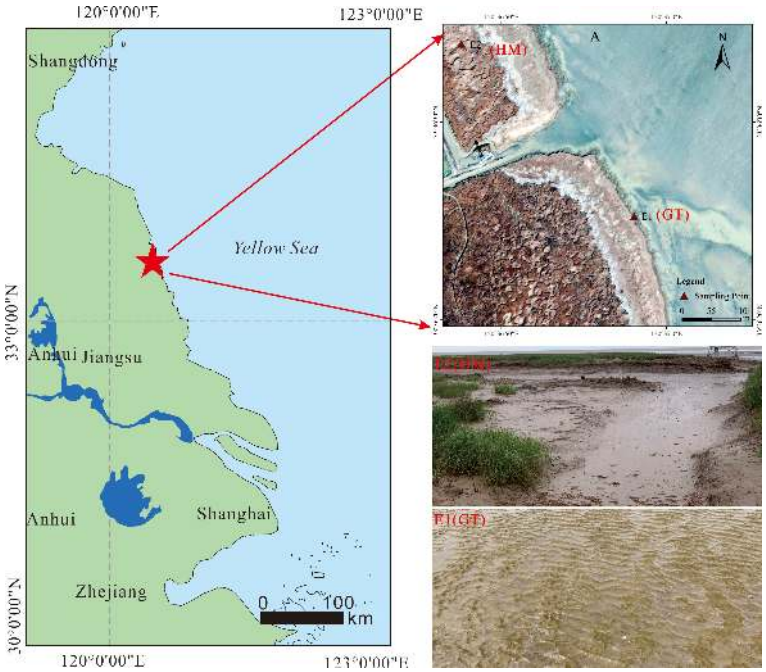


FIGURE 2
Map of sampling locations for the sediment cores.

grain size (Mz), sorting coefficient (σ), skewness (Sk), and kurtosis (KG) were calculated (Zhu, 2008).

Total organic carbon (TOC) and total nitrogen (TN) contents were determined in the Marine Chemistry and Sediment Laboratory at the same institution. Freeze-dried samples were acid-treated to remove inorganic carbon and then analyzed using an Elemental Analyzer. The samples were combusted at high temperature, and the resulting gases were separated and detected to obtain the mass percentages of TOC and TN. The relative error for replicate measurements was below 5%.

Sediment geochronology was established via ^{210}Pb and ^{137}Cs radioactive isotope dating, The total ^{210}Pb in marine sediments originates from two primary sources: supported ^{210}Pb produced *in-situ* by the radioactive decay of 226Ra background activity; and excess ^{210}Pb (210Pbex) derived from atmospheric fallout and subsequent scavenging by suspended particles. To ensure analytical accuracy,137Cs and 226Ra standard samples provided by the China Institute of Atomic Energy, and ^{210}Pb standards from the University of Liverpool, were utilized for calibration. The entire experimental procedure was conducted at the Isotope Laboratory of

TABLE 1 **Experimental instruments and equipment.**

Instrument name	Model	Manufacturer
pH Meter	MODEL III	Branks Rand, USA
Analytical Balance	ME204TE	Mettler Toledo, Switzerland
Constant Temperature Water Bath	HH-6	Changzhou Yuexin Instrument Manufacturing Co., Ltd., China
Electric Hot Plate	SC-404-2.4-4	Dongtai Yuejin Electric Appliance Factory, China
High-speed Refrigerated Centrifuge	TGL-16M	Shanghai Luxiang Instrument Co., Ltd., China
Freeze Dryer (Lyophilizer)	FD-1D-5D	Beijing Boyikang Laboratory Instrument Co., Ltd., China
Ultrapure Water System	IQ-7000	Milli-Q (Merck Millipore), USA
Electric Thermostatic Drying Oven	DHG-9240A	Shanghai Jing Hong Laboratory Instrument Co., Ltd., China
Shaking Incubator	ZQLY-180E	Shanghai Zhichu Instrument Co., Ltd., China
Freezer	RC-RD-830HCZ	Haier Smart Home Co., Ltd., China
Laser Diffraction Particle Size Analyzer	Mastersizer2000	Malvern Instruments Ltd., UK
High-Purity Germanium Gamma Spectrometer	ORTEC-GWL-120-15	EG&G ORTEC, USA
CN Elemental Analyzer	Flash Smart CN	Thermo Fisher Scientific, USA
AAS	Hitachi Z-2000	Hitachi High-Tech Corporation, Japan
ICP-OES	Thermo iCAP 6000	Thermo Fisher Scientific, USA

the Nanjing Institute of Geography and Limnology, Chinese Academy of Sciences. Radionuclide activities were measured using a gamma spectrometer equipped with a GEM high-purity germanium detector, a DSPEC-jr digital spectrometer, and an ORTEC multi-channel analysis system. To ensure data reliability, a 40,000 s measurement cycle was implemented, using the count rate-error ratio correction method for activity calculations.

Major and trace elements were analyzed following acid digestion of the samples. Given the siliceous nature of the samples, an acid dissolution method was employed. To remove the carbonate phase and adsorb seawater Na and K from the bulk samples, approximately 1 g of each sample was placed into a 15 mL centrifuge tube, followed by the addition of 10 mL of deionized water. The centrifuge tube was then placed in a constant-temperature shaking incubator (35 °C) and shaken for 3 hours. After that, the tube was centrifuged at 2200 rpm for 6 minutes, and the supernatant was removed. The above experimental procedure was repeated several times, and a salinometer was used to ensure effective removal of K and Na from seawater. The samples were then dried in an oven at 80 °C. Exactly 100 mg of the dried sample was accurately weighed and placed into a beaker. Subsequently, 5.0 mL of concentrated hydrochloric acid, 3.0 mL of concentrated nitric acid, 8.0 mL of hydrofluoric acid, and 0.25 mL of perchloric acid solution were added in sequence. The beaker was then heated on a hot plate until the solution was completely evaporated to dryness. The residue was then converted into a nitric acid medium using 3% HNO_3 and diluted 2000 times. Finally, measurements were conducted using a Thermo iCAP 6000 series ICP-OES at the Key Laboratory of Surface Geochemistry, Ministry of Education (Nanjing University). Quality control was ensured by repeated analysis of the rock standard reference material BHVO-2(Basaltic powder geological reference material certified by USGS), with the relative standard deviation (RSD) for all elements maintained below 5%.

Iron speciation analysis was performed to extract and quantify functionally distinct iron phases, including total iron (Fe_T), carbonate-associated iron (Fe_{carb}), oxide-bound iron (Fe_{ox}), magnetite-bound iron (Fe_{mag}), and pyrite-associated iron (Fe_{py}),highly reactive iron(Fe_{HR}), $Fe_{HR=}Fe_{carb+}Fe_{ox+}Fe_{mag+}Fe_{py}$ (Poulton and Canfield, 2005). The experimental procedure comprised three parts: (1) The sequential extraction method developed by Poulton and Canfield (Poulton and Canfield, 2005) was utilized to isolate the Fe_{carb}、Fe_{ox}、Fe_{mag} fractions. The specific steps and reagents are as follows: ①Carbonate-associated iron (Fe_{carb}) was extracted by shaking samples with 1 M sodium acetate (buffered to pH 4.5 with acetic acid) at 50 °C for 48 h. ②Easily reducible oxides (Fe_{ox}), including ferrihydrite and lepidocrocite, were targeted using a sodium dithionite solution buffered to pH 4.8 with sodium citrate and acetic acid for 2 h. ③Magnetite (Fe_{mag}) was isolated using an ammonium oxalate acid solution (pH 3.2) for 6 h. (2) The Fepy fraction was extracted via the chromium reduction method. (3) FeT was determined following complete acid digestion. The related experiments were carried out at the Nanjing Institute of Geology and Palaeontology, Chinese Academy of Sciences; the School of Environmental Studies, China University of Geosciences (Wuhan); and the Key Laboratory of Surface Geochemistry, Ministry of Education (Nanjing University), respectively.

3 Results

3.1 Sediment grain size distribution

Sediment grain size classification commonly follows internationally recognized schemes such as those by Shepard and Folk (Folk, 1971). In this study, sediment nomenclature is determined according to the Folk classification system. The Folk method provides a quantitative advantage by categorizing sediments through sand abundance levels (10%, 50%, and 90%) and specific silt-to-clay proportions. This nomenclature system is fundamentally rooted in sedimentary dynamics; for instance, defining "mud" as having <10% sand and a 2:1 to 1:2 silt/clay ratio allows for a deeper interpretation of energy regimes, leading to its broad application in coastal geological studies.

The grain size parameters for core GT are presented in Table 2. The mean grain size (Mz) ranges from 4.02 to 5.87 Φ (average 4.76 Φ), exhibiting an overall trend of first decreasing and then increasing from the bottom upwards. The sorting coefficient (σ) varies between 1.20 and 2.01 (average 1.55), indicating poorly sorted sediments. Skewness (Sk) values range from 0.63 to 3.08 (average 1.94), showing a strongly positively skewed distribution. Kurtosis (KG) falls between 2.37 and 14.06 (average 6.77), suggesting a very narrow peak in the distribution. The vertical variations of these parameters are illustrated in Figure 3.

The grain size characteristics for core HM are summarized in Table 2. The mean grain size (Mz) shows a considerable range (4.16–10.81 Φ, average 6.07 Φ) and displays a distinct coarsening trend from the bottom to the top of the core. This trend reflects continuous accretion on the tidal flat and its progression toward an equilibrium profile. The sorting coefficient (σ) ranges from 0.86 to 3.98 (average 1.62), also indicating poor sorting. Skewness (Sk) varies between -0.85 and 2.05 (average 0.65), predominantly showing positive skewness. Kurtosis (KG) values are between 2.28 and 11.90 (average 4.40), likewise characterizing a narrow peak. The vertical distributions of the grain size parameters are detailed in Figure 3.

3.2 Distribution characteristics of TOC, TN, and C/N in sediments

The analytical results for Total Organic Carbon (TOC), Total Nitrogen (TN), and the resulting C/N ratios for the sediment cores are illustrated in Figure 4.

In core GT, TOC content is relatively low, ranging from 0.021% to 0.240% (mean 0.06%), with values generally fluctuating within this low range. TN content varies between 0.003% and 0.041% (mean 0.019%), showing a fluctuating but overall decreasing trend with depth. The C/N ratio exhibits a wide range from 1.06 to 29.94, with an average of 4.77. Notably, within the 37–71 cm interval, the C/N ratio displays significant fluctuations (1.66-29.94, mean 8.16). An anomalously high value (16.55) occurs at 7 cm depth, while ratios in other sections mostly fall between 1 and 4.

In contrast, TOC content in core HM is significantly higher than in core GT, ranging from 0.075% to 2.376% (mean 0.841%) and exhibiting a distinct upward-increasing trend with depth. TN

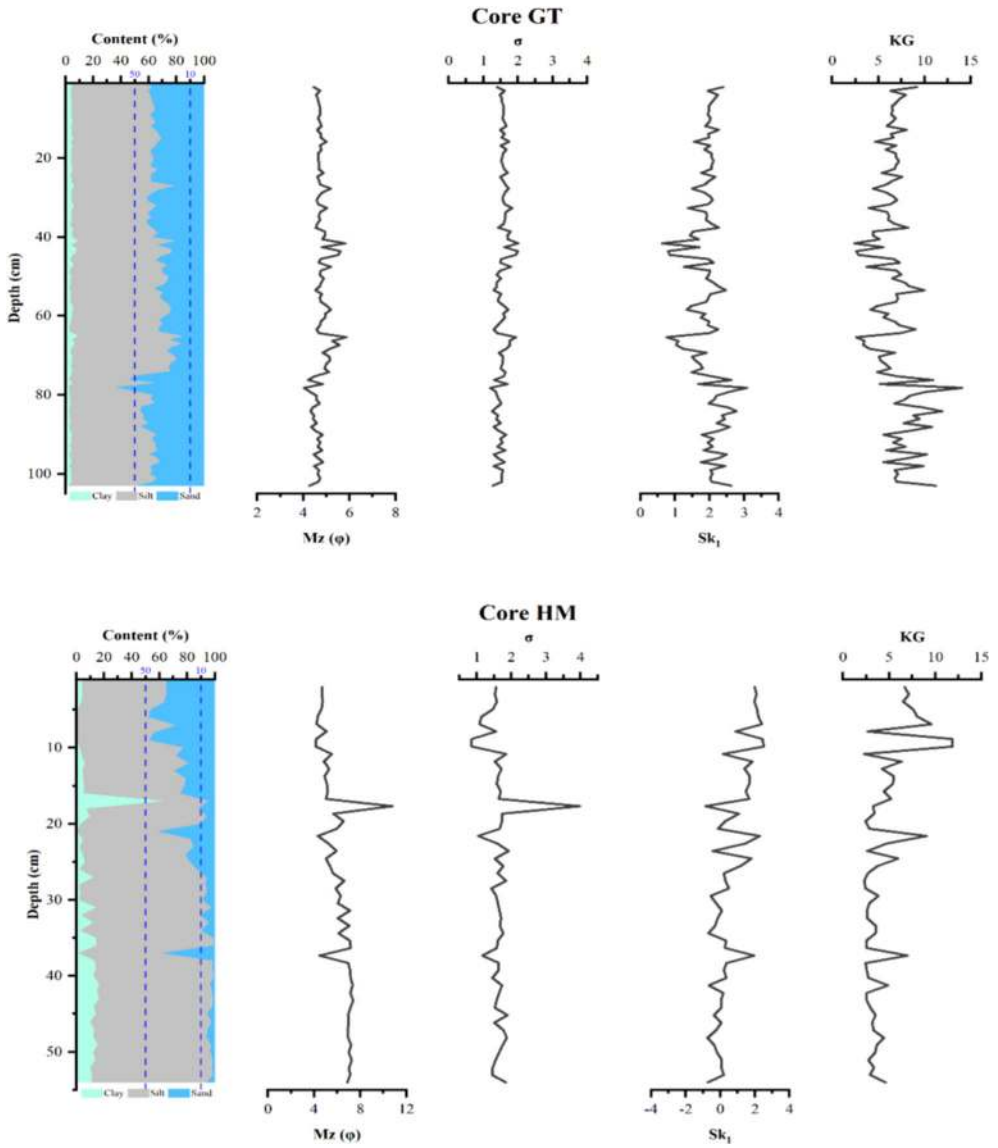


FIGURE 3
Vertical distribution of granulometric parameters in sediment core GT and HM.

content varies from 0.010% to 0.138% (mean 0.071%), similarly increasing with depth. The C/N ratio ranges from 4.89 to 17.24, with a mean of 10.21. Vertically, the C/N ratio shows a fluctuating increase with depth in the 0–34 cm interval, while it transitions to a fluctuating decrease with depth in the 34–54 cm interval.

3.3 Determination of sedimentation rates and geochronology

Sedimentation rates for the two cores were evaluated based on the analytical results of ^{210}Pb and ^{137}Cs radionuclides (Figure 5).

In core GT, ^{210}Pb specific activity ranged from 112.01 to 52.66 Bq/kg (mean 84.91Bq/kg). Conversely,^{137}Cs activities remained consistently below the instrumental detection limit throughout the core profile. This absence may be attributable to post-depositional diffusion, low sedimentary flux within the study area, or instrumental sensitivity constraints; therefore, ^{137}Cs was excluded from the sedimentation rate calculations.

For core HM, ^{210}Pb specific activity varied between 53.01 and 72.89 Bq/kg (mean 64.58 Bq/kg), exhibiting a general decreasing trend with increasing depth. Consistent with the observations in core GT,^{137}Cs activities in core HM were not effectively detected.

In summary, due to the weak ^{137}Cs signal, the geochronological framework in this study was established primarily based on the vertical activity distribution of ^{210}Pb to facilitate the calculation of sedimentation rates.

3.4 Geochemical characteristics of major elements in sediments

This study analyzed ten major elements (Ba, Fe, Mn, Mg, Ca, Ti, Sr, Al, Na, K) in the sediments of cores GT and HM.

The average abundance sequence of these elements is consistent between the two cores, following the order: Na > Al > K > Fe > Ca > Ti > Mg > Ba > Mn > Sr. In core GT, elements such as Fe, Mg, Ca, Ti, Al, Na, and K exhibit relatively higher concentrations, whereas

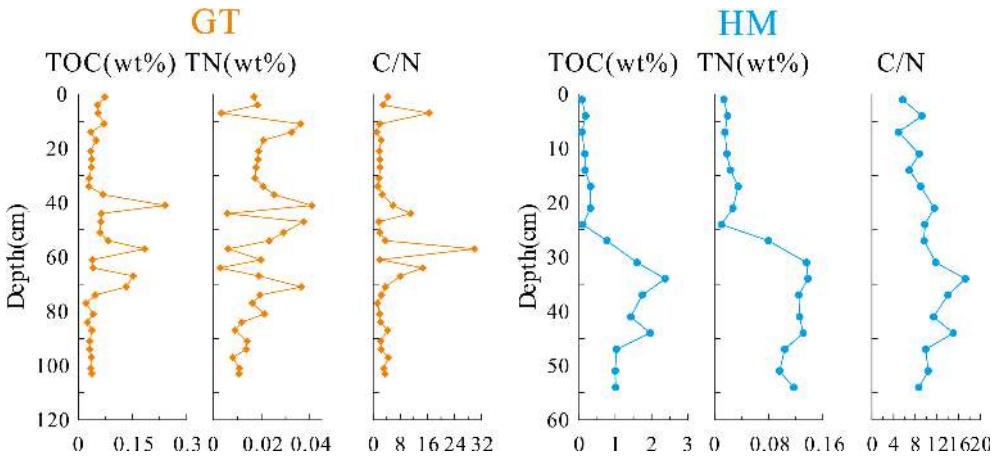


FIGURE 4
Vertical distribution of TOC,TN concentrations and C/N ratios in sediment core GT,HM.

Ba, Mn, and Sr are present in lower amounts. In contrast, core HM shows higher concentrations of Fe, Ca, Al, Na, and K, and lower concentrations of Ba, Mn, Mg, Ti, and Sr.

Regarding their vertical profiles (Figure 6), elements including Fe, Mn, Mg, and Ca in core GT, as well as Fe, Mn, Mg, Ti, and Ca in core HM, display distinct trends with depth. Furthermore, the variations among these elements show a strong co-variation.

The results of the correlation analysis are presented in Table 3 for core GT and Table 4 for core HM.

In core GT, the Pearson correlation coefficients between elements Fe, Mn, Mg, Ca, Ti, and Al are generally low (<0.25), indicating weak associations. In contrast, Ba, Sr, Na, and K show significant positive correlations with Al, with r values of 0.77, 0.61, 0.61, and 0.74, respectively. Most elements (except Fe, Mn, Ca, Ti,

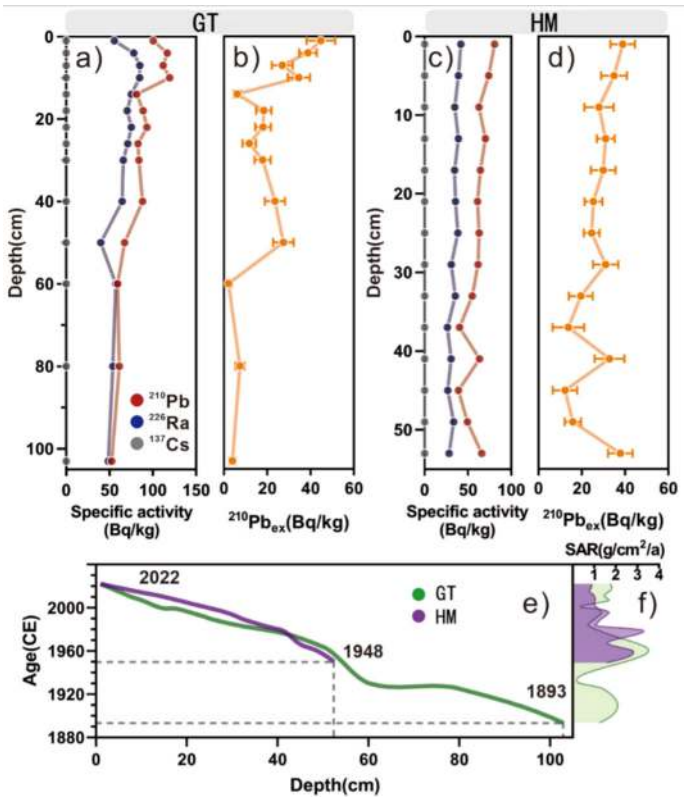


FIGURE 5
Vertical profiles of ^{210}Pbtotal, ^{226}Ra and ^{137}Cs activities in the tidal flat sediment cores. **(a, c)**: The specific activity (Bq/kg) of ^{210}Pbtotal, ^{226}Ra, and ^{137}Cs at various depths (cm) for the GT core and HM core, respectively. **(b, d)**: The specific activity (Bq/kg) of ^{210}Pbexcess ($^{210}Pb_{ex}$) at different depths for the GT core and HM core. **(e)**: The derived Age (CE) versus Depth (cm) relationship curves for both cores (GT and HM). **(f)**: The Sediment Accumulation Rate (SAR; g/cm^2/a) distribution over different historical periods at both sites (GT and HM).

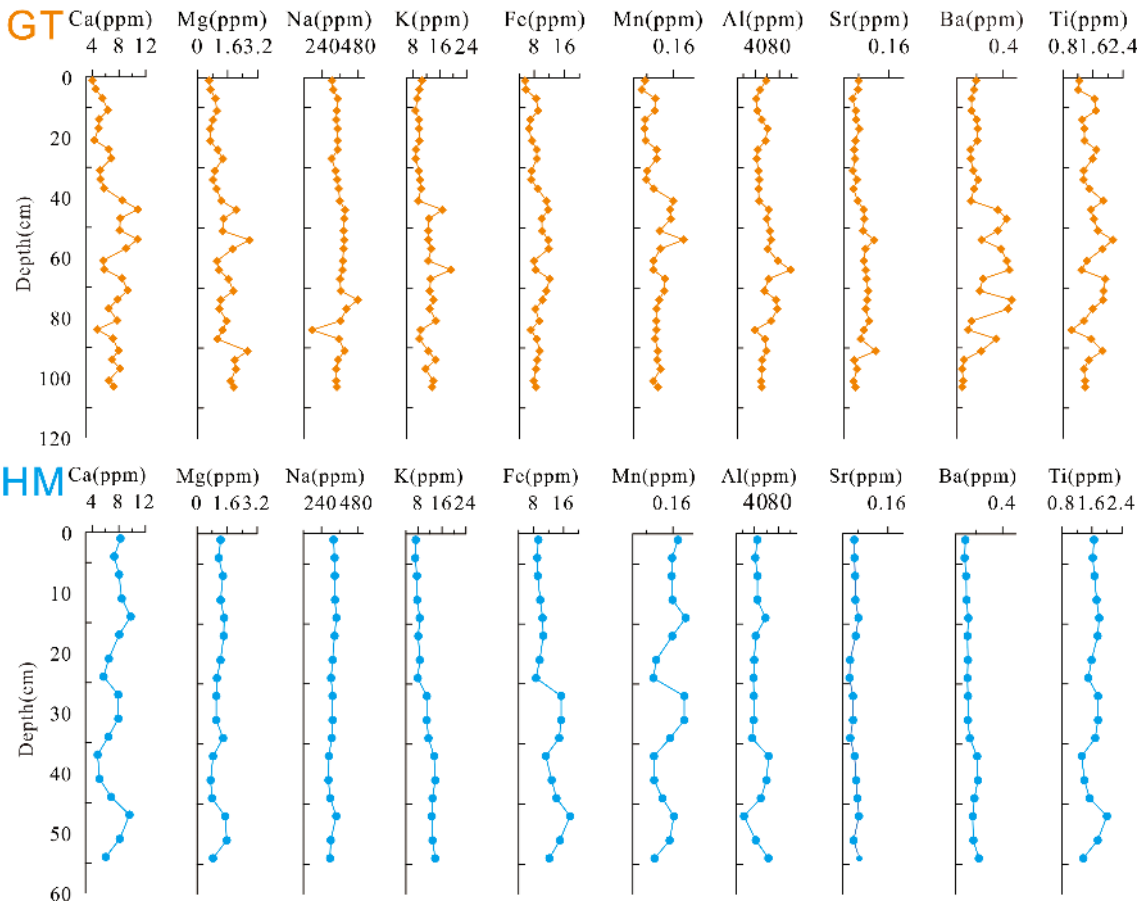


FIGURE 6
Vertical distribution of geochemical element concentrations in sediment core GT,HM.

and Na) exhibit low correlations (r < 0.3) with both the mean grain size and clay content. However, Fe, Mn, Ca, Ti, and Na show relatively higher correlations with these two parameters, with r values approximately around 0.5.

In core HM, Fe, Mn, Mg, Ca, Ti, Na, and K are all negatively correlated with Al. Conversely, Ba, Sr, and K exhibit certain positive correlations with Al, with r values of 0.54, 0.38, and 0.30, respectively. For most elements (except Fe), the correlations with both mean grain size and clay content are low (r < 0.35). In contrast, Fe demonstrates a relatively higher correlation with these two parameters, with an r value of approximately 0.5.

3.5 Iron speciation and vertical distribution in sediments

The distribution of iron species within the two sediment cores following Fe_{ox}>Fe_{mag}>Fe_{carb}> Fe_{py} (Figure 7). The Fe_{HR}/Fe_T ratios ranged from 0.04 to 0.57 (mean 0.38) and the average ratios of Fe_{ox}/Fe_{HR} and Fe_{mag}/Fe_{HR} are 0.51 and 0.37 in core GT. Similarly, in core HM, the Fe_{HR}/Fe_T ratios ranged from 0.22 to 0.57 (mean 0.38) and Fe_{ox}/Fe_{HR} and Fe_{mag}/Fe_{HR} are 0.40 and 0.29, indicating that reactive iron is predominantly present in the Fe^{3+} form, primarily as Fe_{ox} and Fe_{mag}.

Regarding vertical distribution (Figure 8), distinct depth-dependent variations are observed for the different iron phases. In core GT, Fe_{py} shows an overall increasing trend with considerable fluctuation from 0–74 cm before stabilizing below 74 cm. Fe_{carb} remains relatively stable from 0–34 cm, with a minimum value at 11 cm, and then exhibits significant fluctuations characterized by an initial increase followed by a decrease between 34–84 cm, peaking at 67 cm, and stabilizes again below 84 cm. Fe^{ox} content increases steadily with depth with minor fluctuations, reaching its minimum at 11 cm, while Femag displays a steady decreasing trend with depth and minor fluctuations, also showing its lowest value at 11 cm. The Fe_{py}/Fe_{HR} ratio remains below 0.8 throughout the core, and the Fe_{HR}/Fe_T ratio fluctuates around 0.38, with the greatest deviation observed at 11 cm.

In core HM, Fe_{py} increases with depth from 0–44 cm, peaking at 44 cm, then decreases before increasing again from 44–54 cm. Fe_{carb} generally increases with depth overall. Fe_{ox} is stable from 0–27 cm, then decreases before increasing from 27–54 cm, with its highest value at 27 cm. Femag generally increases with depth, showing significant variation and reaching a maximum at 31 cm. The Fe_{py}/Fe_{HR} ratio is predominantly below 0.8 in this core. The Fe_{HR}/Fe_T ratio is below 0.38 from 0–27 cm, above 0.38 from 27–44 cm, and fluctuates around 0.38 from 44–54 cm.

TABLE 2 Distribution of granulometric parameters and component fractions in the sediment cores.

Core	Statistic	Mz(Φ)	σ	SK	KG	Clay (%)	Sand (%)	Silt (%)
GT	Min	4.02	1.20	0.63	2.37	1.76	15.57	34.16
	Max	5.87	2.01	3.08	14.06	9.17	64.08	77.02
	Average	4.76	1.55	1.94	6.77	3.99	34.82	61.18
HM	Min	4.16	0.86	-0.85	2.28	0.10	0.68	32.20
	Max	10.81	3.98	2.50	11.90	62.90	47.90	91.70
	Average	6.07	1.62	0.65	4.40	8.33	15.38	76.29

(Note: Mz, Mean grain size; σ, Sorting coefficient; SK, Skewness; KG, Kurtosis);.

4 Discussion

4.1 Environmental implications of sediment grain size characteristics

Sediment grain size characteristics serve as crucial proxies for identifying and reconstructing the evolution of coastal depositional environments. Distinct sedimentary facies typically correspond to unique grain size assemblages, making grain size analysis a key tool for discriminating depositional settings (Feng et al., 2024b).

The results of this study show that the upper section of core GT (0–44 cm) exhibits a distinct grain-size fining trend, which aligns with the natural progradation of tidal flats toward a low-energy high-marsh equilibrium as surface elevation increases through continuous accretion. However, compared to the adjacent core HM, this fining trend in the GT area is less pronounced. This disparity is primarily attributed to the gradual degradation of Spartina alterniflora following its initial introduction, resulting in a persistently low vegetation density that weakened its biological trapping capacity for fine-grained suspended sediments. Conversely, the coarsening trend observed in the lower section (44–103 cm) profoundly records the anthropogenic forcing of large-scale land reclamation in the 1960s. These engineering projects forced the narrowing of tidal channels and significantly intensified local tidal current velocities, thereby enhancing the winnowing and screening of fine-grained materials and disrupting the natural sedimentary fining sequence.

Core HM presents a continuous coarsening-upward sequence from bottom to top. This feature is the result of the synergistic interplay between regional natural evolution and biological trapping effects. On the one hand, this regressive sequence indicates a shift from a distal, low-energy facies to a more proximal, higher-energy facies as the shoreline advanced seaward. On the other hand, with the timing of the introduction of Spartina alterniflora to the Jiangsu coast in 1982 (Feng et al., 2024a). Spartina alterniflora, characterized by its dense canopy and extensive root systems, significantly enhances the attenuation of near-surface flow, thereby facilitating the settlement of fine-grained suspended matter. This superimposed effect renders the fining trend in core HM more pronounced than that in core GT and accounts for its higher average sedimentation rate. Notably, a marked shift in sediment composition is observed at the 17 cm depth, characterized by a sharp decrease in silt content, a significant increase in clay content alongside peaks in mean grain size and sorting coefficient and relatively stable sand content. The chronological framework established by ^{210}Pb and ^{137}Cs confirms that this interval represents the late 1990s, precisely coinciding with the historical landfall of Winnie, one of the most powerful typhoons to affect the Abandoned Yellow River Delta in the 20th century. Furthermore, the shoreline-stabilizing function of *S. alterniflora* can mitigate

TABLE 3 Correlation analysis between geochemical elements and grain-size fractions in sediment core GT.

Variables	Ba	Fe	Mn	Mg	Ca	Ti	Sr	Al	Na	K	Mz/Φ	Clay/%
Ba	1											
Fe	0.31	1										
Mn	0.19	0.86	1									
Mg	-0.05	0.65	0.72	1								
Ca	0.24	0.91	0.89	0.80	1							
Ti	0.27	0.84	0.72	0.51	0.74	1						
Sr	0.54	0.51	0.50	0.55	0.55	0.46	1					
Al	0.77	0.21	0.14	0.11	0.21	0.14	0.61	1				
Na	0.63	0.53	0.34	0.24	0.51	0.63	0.41	0.61	1			
K	0.45	0.39	0.32	0.49	0.46	0.08	0.50	0.74	0.45	1		
Mz/Φ	0.26	0.68	0.57	0.21	0.59	0.57	0.18	0.10	0.40	0.15	1	
Clay/%	0.10	0.49	0.46	0.08	0.43	0.45	-0.01	-0.08	0.27	-0.06	0.94	1

10.3389/fmars.2026.1800486

TABLE 4 Correlation analysis between geochemical elements and grain-size fractions in sediment core HM.

Variables	Ba	Fe	Mn	Mg	Ca	Ti	Sr	Al	Na	K	Mz/Φ	Clay/%
Ba	1											
Fe	0.44	1										
Mn	-0.59	0.23	1									
Mg	-0.51	0.01	0.50	1								
Ca	-0.51	0.17	0.84	0.72	1							
Ti	-0.52	0.38	0.80	0.77	0.90	1						
Sr	0.42	0.18	0.12	-0.08	0.35	0.08	1					
Al	0.54	-0.32	-0.38	-0.57	-0.46	-0.74	0.38	1				
Na	-0.71	-0.16	0.70	0.71	0.86	0.79	0.20	-0.50	1			
K	0.92	0.73	-0.35	-0.43	-0.38	-0.29	0.31	0.30	-0.67	1		
Mz/Φ	0.26	0.46	0.11	0.05	0.12	0.21	0.29	-0.09	-0.08	0.33	1	
Clay/%	0.04	0.14	0.12	0.13	0.15	0.20	0.23	-0.07	0.08	0.03	0.92	1

scouring by storm surges, favoring the retention of coarser particles and thus buffering, to some extent, the dramatic geomorphic reshaping of tidal flats by extreme climatic events.

In summary, the vertical variations in grain size within the tidal flat cores of the Abandoned Yellow River Delta archive the combined effects of multiple environmental drivers. Human reclamation altered tidal flat geomorphology and flow patterns, storm surges and tidal processes reshaped the tidal flat surface, and *S. alterniflora* enhanced the deposition of fine-grained sediments through its sediment-trapping effect. The superimposed influences of these natural and anthropogenic factors collectively drive the progradation of the silt-mud tidal flat, ultimately recorded in the vertical profile of sediment grain size characteristics.

4.2 Controls on organic matter distribution and environmental implications

The C/N ratio in sediments acts as a robust proxy for discriminating organic matter provenance (terrestrial versus marine) (Li et al., 2016; Yang et al., 2024). By contrasting the C/N signatures of the bare flat (GT) and the *Spartina alterniflora* marsh (HM) cores, this study reveals differences in organic matter input and preservation mechanisms under distinct sedimentary environments.

Most C/N ratios in core GT are below 5 (Figure 9), indicating that its organic matter is primarily derived from marine sources such as phytoplankton, resulting in an overall low content. For samples with TOC/TN ratios exceeding 10, the results suggest a significant contribution from terrestrial plant debris or soil organic matter delivered via fluvial transport, potentially exacerbated by anthropogenic activities. Furthermore, the preferential mineralization of organic matter within the sediments—where nitrogen-rich compounds are often degraded more rapidly—may also account for the elevated TOC/TN ratios. Collectively, these factors, modulated by shifts in the depositional environment or biological mediation, drive the observed stoichiometric variations in the organic carbon and nitrogen pools. For example, research by Yang et al. (2024) on the organic matter provenance in Ross Sea sediments indicated that TOC/TN ratios exceeding 12 generally signify a substantial input of terrestrial organic matter, such as plant debris and soil organic matter (Yang et al., 2024). Furthermore, studies by Gebert and

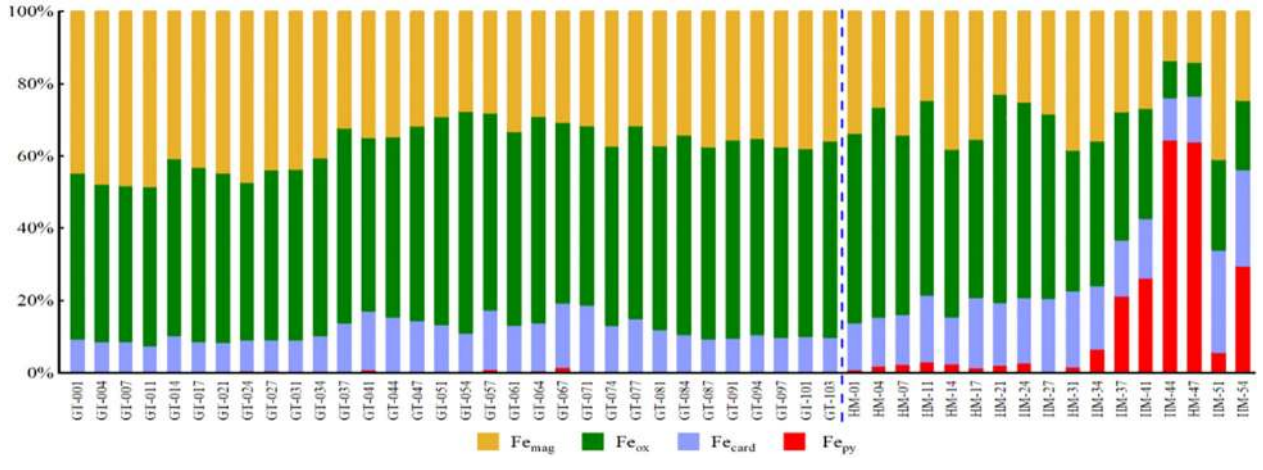


FIGURE 7
Cumulative percentage proportions of Fe_{mag},Fe_{ox},Fe_{carb} and Fe_{HR} in the sediment cores.

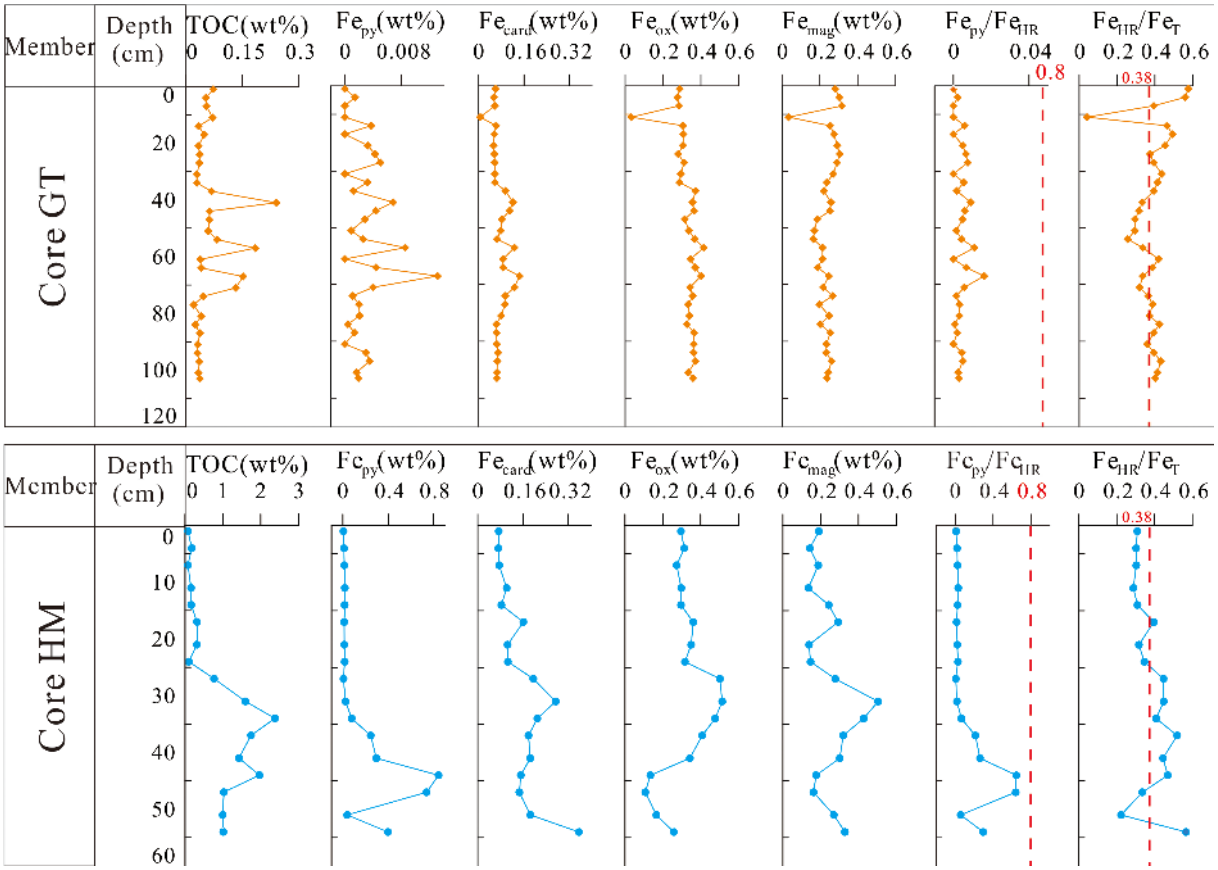


FIGURE 8
Vertical distribution profiles of iron species in sediment core GT、HM.

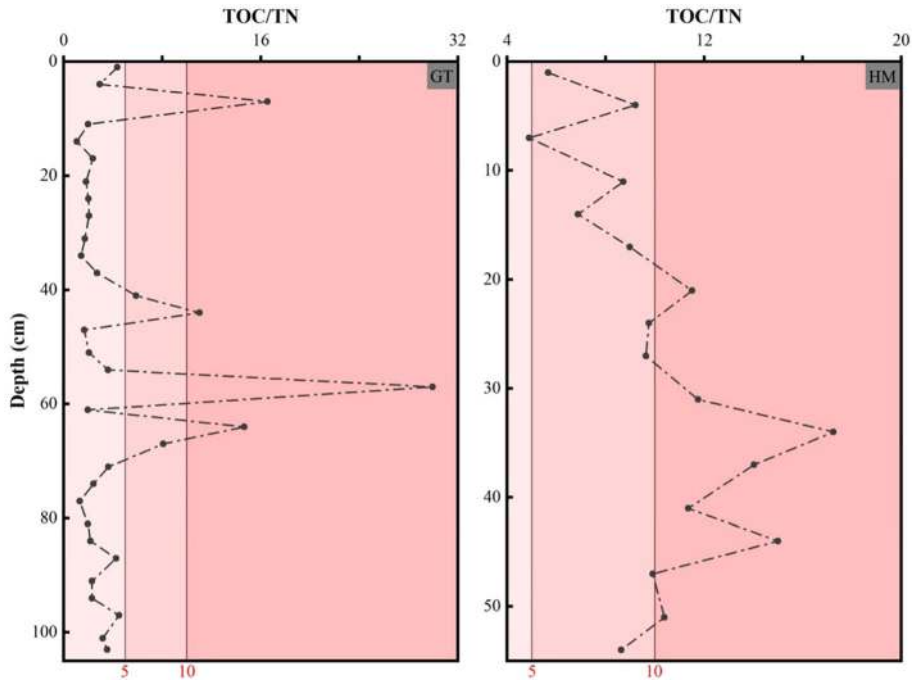


FIGURE 9
Provenance of organic matter in the tidal flat sediment cores.

Zander (2024) confirmed that under anaerobic conditions, the mineralization of organic matter is suppressed, which subsequently leads to an elevation in TOC/TN ratios (Gebert and Zander, 2024). Therefore, anomalously high values (with a maximum C/N of 29.94) occur within the 37–71 cm interval. This likely reflects a period of strong pulsed input of terrigenous organic matter (Feng et al., 2024a) or may be associated with the redistribution of surface soils due to nearby human engineering activities. This also indirectly suggests that the depositional environment during this period likely shifted toward suboxic or anoxic conditions, which in turn facilitated the anomalous elevation of TOC/TN ratios.

In contrast, C/N ratios in core HM are generally above 10, suggesting a predominance of terrigenous organic matter input. The significant increase in TOC content with depth not only reflects the contribution of plant biomass following the introduction of *S. alterniflora* but also indicates the effective trapping and accumulation of terrigenous organic carbon by the vegetation. Notably, within the upper 20 cm, the C/N ratio decreases to below 10. This may be related to a reduction in vegetation coverage and consequent decrease in organic matter input, potentially caused by artificial management or natural degradation of *S. alterniflora* (Feng et al., 2024a). Furthermore, this process is influenced by large-scale land reclamation and seawall advancement, which have not only altered the hydrodynamic environment but also physically severed the ecological connectivity between the tidal flat and the land. At the HM site, habitat changes following reclamation and artificial management have cut off the supply of terrestrial organic matter. This shift in organic matter provenance is likely the fundamental mechanism underlying the transition of C/N ratios from terrestrial signatures (>10) to marine signatures (<10) in the surface layers. Beyond these influences, variations in TOC/TN ratios may also be modulated by the depositional environment. For instance, in the muddy area of the Central Yellow Sea Shelf, the association of iron oxides with organic carbon can effectively enhance resistance to microbial degradation, thereby facilitating the long-term preservation of organic carbon (Wei et al., 2024).

In summary, the C/N ratios clearly indicate a fundamental difference in organic matter sources between the GT and HM sediments: the former is dominated by marine sources, while the latter is primarily terrigenous and is significantly influenced by vegetation evolution and human activities.

4.3 Sedimentation rate analysis based on geochronology

The geochronological framework established via ^{210}Pb and ^{137}Cs dating reveals mean sedimentation rates of 1.25 cm/a for the GT core and 1.39 cm/a for the HM core. These values align well with previous regional studies while exhibiting distinct spatial heterogeneity (Wang et al., 2005; Li et al., 2010).

The detailed analysis of the vertical evolution of sedimentation rates in the cores reveals a consistent pattern: the sedimentation rate generally decreases as tidal flat accretion progresses. This phenomenon aligns closely with the historical geomorphological evolution of the Abandoned Yellow River Delta tidal flats under the influence of intensive anthropogenic activities, such as land reclamation, over recent decades. The sediment supply to this coastal region is primarily governed by the North Jiangsu Coastal Current, which redistributes relict Yellow River materials. The NJCC exhibits significant seasonal dynamics: in summer, it is driven northward by the prevailing southeast winds; in winter, observations indicate a northward flow that originates from the Yangtze River estuary and extends to the waters south of the Abandoned Yellow River mouth. In conjunction with these hydrodynamic processes, large-scale land reclamation and the seaward advancement of seawalls have forced the active tidal flat system to migrate offshore. Since Core GT is situated at the western margin of this depositional zone, the seaward migration of the active depocenter has resulted in a progressive decline in the average sedimentation rate at this specific location. This transition from an active depocenter to a more stable, landward tidal flat environment effectively explains the decreasing sedimentation rates recorded in the geochronological data.

Notably, a significant peak in sedimentation rate (reaching up to 3.24 cm/a) is identified for the period 1979–1986, coinciding with the widespread introduction and expansion of *Spartina alterniflora*. This finding quantitatively confirms the substantial acceleration of tidal flat sedimentation driven by the sediment-trapping effect of *S. alterniflora* (Fan et al., 2024).

4.4 Environment implications of major element distributions

Pearson correlation analysis revealed that the correlation coefficients between most geochemical elements (with the exception of Fe, Mn, Ca, and Ti) and the mean grain size or clay content were below 0.3, indicating a weak statistical relationship. In contrast, Fe, Mn, Ca, and Ti exhibited correlation coefficients approaching 0.5, suggesting a relatively robust correlation with both mean grain size and clay content. These significant associations imply that elements such as Ba, Fe, Mn, Mg, Ca, Ti, Sr, Na, and K are well-coupled with terrigenous components like Al and clay minerals. This suggests that the fluctuations in these elements are, to a certain extent, governed by terrestrial material input and the adsorption effects associated with fine-grained particles (Qian et al., 2002). The differences in element-grain size correlations between the GT and HM cores fundamentally stem from their distinct sediment compositions: core GT is dominated by silt and sand, whereas core HM is primarily composed of silt. Notably, the correlation between Sr and grain-size parameters was not significant, which is inconsistent with the typical grain-size effect. This suggests that the distribution of Sr in tidal flats may be influenced by complex factors, such as the presence of biogenic fragments (e.g., shells and foraminifera) or variations in mineral composition. The specific accumulation mechanisms for Sr require further investigation to be fully elucidate (Xu et al., 2009).

In core GT, elements like Fe, Ca, and Mn exhibit highly synchronous vertical trends ($r > 0.5$), indicating consistent geochemical behavior. Variations in their concentrations align closely with changes in clay and silt content as well as mean grain size. This suggests that their distribution is not only governed by terrigenous input and particle adsorption but also sensitively responds to phased shifts in sedimentary dynamics and environmental conditions.

The vertical distribution of major elements in core HM displays a distinct two-stage pattern. The section below 40 cm is characterized by higher silt content, stable Fe concentrations (predominantly high reactive iron), and elevated TOC. This suggests that the coupling of iron oxides and organic carbon effectively facilitated long-term TOC preservation, while also reflecting a relatively high-energy yet stable depositional environment. Conversely, the upper section (above 40 cm) undergoes significant sediment fining, evidenced by a decrease in mean grain size and a relative enrichment of Mn and Ca. The concomitant decrease in TOC content in this layer is likely driven by the increased relative proportion of mineral components. This shift corresponds to both decadal-scale reclamation activities and the recent degradation of Spartina alterniflora, which synergistically enhanced the trapping and retention efficiency of fine-grained materials, thereby reshaping the tidal flat sedimentary dynamics and elemental enrichment patterns. Notably, the abrupt increase in TOC at approximately 20 cm is associated with the 1982 introduction of S. alterniflora, as discussed in the preceding sections.

4.5 Environment implications of major element distributions

4.5.1 Source of iron and controlling mechanisms of sedimentary iron

In the tidal flat sediment cores of the Abandoned Yellow River Delta, the average Total Iron Fe_T content reaches 1.94%, which approaches the average Fe_T levels reported for global shelf-edge marine sediments (2.92 ± 0.78%). This suggests that the sources of Fe_T are likely modulated by the dual influence of terrestrial material input and marine environmental conditions (Peng et al., 2014). Furthermore, the grain size distribution in this region is complex; notably, the fine-grained fractions, such as clay, exhibit a significant correlation with Fe_T content. A significant positive correlation between Fe_T and Al (R^2 = 0.80) aligns with the elemental stoichiometry of global riverine suspended particulates (Figure 10A, R^2 = 0.90) (Poulton and Raiswell, 2002), indicating terrestrial riverine discharge as the primary source of iron in these tidal flats. Furthermore, a positive correlation is also observed between Fe_T and highly reactive iron (Fe_{HR}) (Figure 10B, R^2 = 0.34), providing additional support for their shared terrigenous origin.

To better characterize the provenance of iron, this study examined the relationship between Fe_T content and the Fe_{HR}/Fe_T ratios across different sedimentary environments (Figure 10D). The results show that data points from the study area cluster near the distribution fields of shelf margin sediments and Yellow River particulates, and follow a trend similar to that of global riverine samples (Poulton and Raiswell, 2002). Additionally, the robust correlation between Fe_T and clay content (Figure 10C, R^2=0.62) indicating that adsorption and enrichment by fine-grained particles are key mechanisms controlling iron distribution. According to previous studies, the tidal flat sediments in the Abandoned Yellow River Delta of northern Jiangsu primarily originate from terrestrial inputs of surrounding rivers. Significant sediment fluxes from the Old Yellow River, Sheyang River, and Guan River are discharged into the coastal zone and subsequently deposited on the tidal flats (Xiang et al., 2024). Furthermore, suspended particulate matter from the Yangtze River is transported northward to the northern Jiangsu coast during winter via the northward coastal current, further modulating the regional sediment distribution. Simultaneously, the transport and redistribution processes driven by the Northern

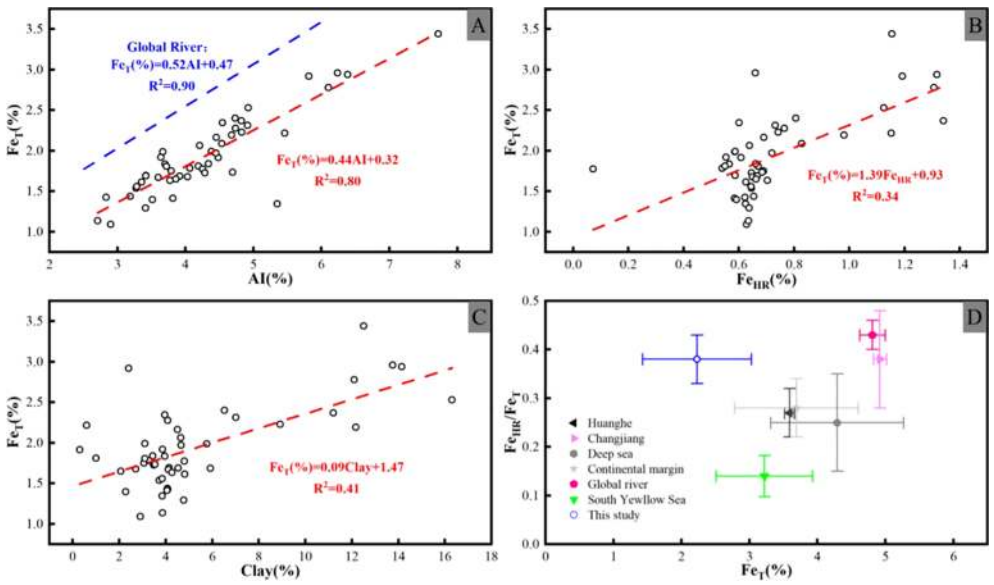


FIGURE 10
Provenance indicators of iron in the tidal flat sediments. **(A)** Correlation between total iron Fe_T and aluminum Al in the study area compared with global riverine particulates, global riverine data adapted from Poulton and Raiswell (Poulton and Raiswell, 2005);**(B)** Correlation between Fe_T and highly reactive iron Fe_{HR} in the sediment cores. **(C)** Correlation between Fe_T and clay content. **(D)** Cross-plot of Fe_{HR}/Fe_T ratios versus Fe_T concentrations across diverse sedimentary environments. Comparative data sources include: global continental margin and deep-sea sediments from Raiswell and Canfield (Raiswell and Canfield, 1998), Yellow River, Yangtze River, and global riverine particulates from Poulton and Raiswell (Poulton and Raiswell, 2002), and surface sediments of the South Yellow Sea from Ma et al (Ma et al., 2018).

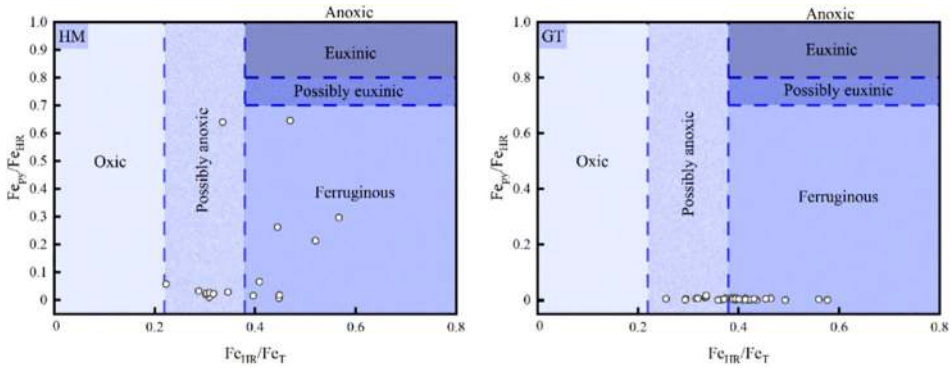


FIGURE 11
Cross-plot of iron speciation ratios (Fe_{py}/Fe_{HR}-Fe_{HR}/Fe_T) in the tidal flat sediment cores.

Jiangsu Coastal Current exert a critical influence on the enrichment and spatial patterns of these sediments (Zhang et al., 2018). Integrating the Fe_{HR}/Fe_T ratios with the regional geological context, it can be concluded that the iron in the tidal flat sediments of the Subei Abandoned Yellow River Delta is primarily sourced from the ancient Yellow River and surrounding river inputs, with its distribution further modulated by the reworking and transport actions of the Subei Coastal Current.

4.5.2 Iron speciation and its indication of oxidative environments

Iron speciation analysis is a common method for identifying redox conditions in sedimentary environments (Gilleaudeau and Kah, 2015; Li et al., 2015). In this study, the mean Fe_T/Al ratio of 0.46 falls well within the range characteristic of typical oxic to suboxic regimes. However, diagnostic cross-plots utilizing Fe_{py}/Fe_{HR} versus Fe_{HR}/Fe_T (Figure 11) reveal interpretative discordances. Pasquier et al. (2022) observed a mismatch between the actual redox status and the redox conditions inferred from iron speciation across various depositional environments (Han et al., 2023). For instance, Boyko et al. (2019) found that in the Gulf of Aqaba (Red Sea), the delivery of substantial aeolian FeHR is a primary driver for the elevated FeHR/FeT ratios in deep-water sediments (Boyko et al., 2019).

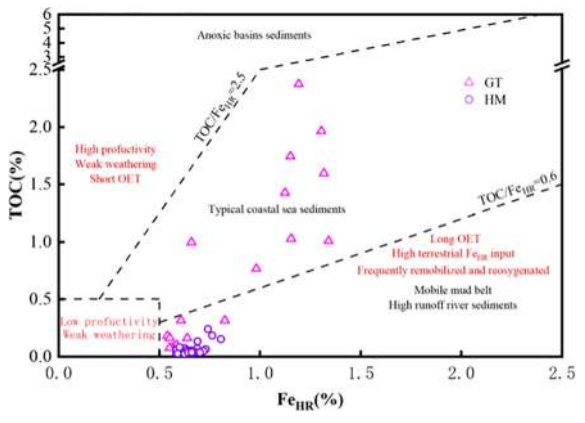


FIGURE 12
Relationship between TOC and FeHR concentrations in the tidal flat sediment cores; OET denotes Oxygen Exposure Time.

Analysis suggests that the generally high Fe_{HR}/Fe_T ratios (>0.22) in this region do not solely reflect redox conditions but are also influenced by intense chemical weathering, terrestrial runoff and sea-level fluctuations. The iron in the tidal flat sediment cores of the Abandoned Yellow River Delta primarily originates from terrigenous iron transported by surrounding rivers. This region is situated in a warm temperate humid monsoon climate zone, which facilitates active chemical weathering. This process leads to the leaching and loss of soluble elements from rock minerals, such as Na, K, and Ca, while insoluble elements (e.g., Al and Fe) become relatively enriched. Specifically, during this weathering process, iron typically forms insoluble mineral phases—primarily iron oxides—which adhere to the surfaces of parent rock minerals (Martin and Meybeck, 1979; Canfield, 1997). Consequently, this leads to a significant elevation in both the Fe_{HR} content and the Fe_{HR}/Fe_T ratios within the riverine sediments (Poulton and Raiswell, 2002; Martin and Meybeck, 1979; Canfield, 1997).Furthermore, under the warm-temperate humid climate, labile elements are leached away, leading to the relative enrichment of reactive iron on particle surfaces (Vosteen et al., 2022). This process results in an elevated baseline value for this ratio.

Huang et al., by synthesizing global data, categorized the relationship between total organic carbon (TOC) and Fe_{HR} into four distinct patterns (Figure 12) (Huang et al., 2023), offering a new perspective for understanding their coupled behavior in sediments. In this study, most tidal flat sediments exhibit TOC/Fe_{HR} ratios below 0.6,instead, a subset of samples exhibits TOC/Fe_{HR} ratios falling within the range of 0.6 to 2.5. This phenomenon not only reflects the influence of high Fe_{HR} influx from fluvial delivery but also underscores that the oxic and suboxic depositional environments within the study area significantly facilitated TOC mineralization. Such conditions are fundamentally unfavorable for the burial and long-term preservation of organic carbon. Furthermore, this stoichiometric relationship suggests that Fe_{HR} and TOC likely share a common provenance.

Over the past century, the Jiangsu coast has experienced a persistent sea-level rise at a rate of approximately 3.35 mm/a (He et al., 2020).This transgression has effectively accelerated the seaward export and subsequent redeposition of iron-rich coastal

colloids, thereby augmenting the loading of the Fe_{ox} fraction within the sedimentary sink. Consequently, this hydro-geochemical process acts as an objective confounding factor, constraining the interpretive precision of iron speciation when utilized as a paleo-environmental proxy.

5 Conclusion

Based on sediment cores collected from the bare flat (GT) and the *Spartina alterniflora* zone (HM) in the Yancheng coastal wetlands of Jiangsu Province, this study employed a multi-proxy approach integrating grain size, organic geochemistry, elemental geochemistry, iron speciation, and ^{210}Pb-^{317}Cs dating. This analysis reveals the sedimentary environmental evolution and its primary controlling factors over the past century in the silt-mud tidal flats of the Abandoned Yellow River Delta. The main conclusions are as follows:

(1) Sediment grain size records the evolution of multi-scale dynamic environments. Core GT (mean grain size: 4.76 Φ, sandy silt) exhibits a "coarse-fine-coarse" vertical sequence, responding to early-stage enhanced hydrodynamics due to reclamation and later-stage sediment fining induced by the sediment-trapping effect of introduced *S. alterniflora*. In contrast, core HM (mean grain size: 6.07 Φ, predominantly silt) shows a continuous "coarsening-upward" sequence, reflecting the natural progradation of the tidal flat and its progression toward an equilibrium profile.

(2) Organic matter sources show distinct habitat differentiation. The C/N ratios in core GT are mostly below 5, indicating a predominance of marine-derived organic matter. Conversely, core HM exhibits C/N ratios mostly above 10, demonstrating significant terrigenous characteristics. The increase in TOC and TN content with depth in core HM confirms the interception and accumulation of terrigenous organic matter by *S. alterniflora*.

(3) Sedimentation rates reveal the superimposition of natural and anthropogenic influences. Based on the ^{210}Pb chronological framework, the average sedimentation rates for GT and HM are 1.25 cm/a and 1.39 cm/a, respectively. The overall declining trend with tidal flat progradation reflects the regulatory effects of seawall advancement and variations in the coastal current on sediment deposition patterns. A significant peak in sedimentation rate during the initial introduction period of *S. alterniflora* (1979–1986) quantitatively confirms its bio-sedimentation effect.

(4) The distribution of major elements is jointly controlled by the "grain-size effect" and sediment provenance. Elements such as Fe, Mn, Ca, and Ti show significant positive correlations with clay content, indicating their enrichment is primarily governed by adsorption onto terrigenous fine particles. The decoupling of elements like Sr from grain-size parameters suggests their distribution is influenced by biological or authigenic processes. The differences in element-grain size correlations between cores GT and HM further demonstrate how sediment composition modulates elemental geochemical behavior.

(5) Iron speciation reflects complex land-sea interactions and redox conditions. Sedimentary iron species are dominated by Fe_{ox}, which increases with depth. Fe_T concentrations approximate the background values of continental margin sediments and correlate significantly with Al, indicating a primary terrestrial riverine derivation. The elevated Fe_{HR}/Fe_T ratios are largely inherited from weathering products in the catchment and are modulated by chemical weathering, runoff, and sea-level changes, rendering them unreliable as a standalone *in-situ* redox proxy. The study area is characterized by an oxic-to-suboxic environment; relatively low TOC/Fe_{HR} ratios suggest that reactive iron likely promotes the mineralization of organic carbon, thereby constraining its potential for long-term burial and preservation.

In summary, the sedimentary evolution of the tidal flats in the Abandoned Yellow River Delta results from the combined effects of natural dynamics (tides, storm surges, coastal currents) and human activities (reclamation, vegetation introduction). The integrated multi-proxy analysis provides an effective approach for deciphering environmental changes in such land-sea interaction zones and offers a scientific basis for regional tidal flat resource management and carbon cycle assessment.

Data availability statement

The original contributions presented in the study are included in the article/supplementary material. Further inquiries can be directed to the corresponding authors.

Author contributions

ZZ: Writing – original draft, Writing – review & editing. HW: Writing – original draft, Funding acquisition, Writing – review & editing. QL: Writing – review & editing, Investigation, Data curation. XT: Data curation, Writing – review & editing. HZ: Writing – review & editing, Investigation, Methodology. DL: Data curation, Methodology, Supervision, Writing – review & editing.

Funding

The author(s) declared that financial support was received for this work and/or its publication. The research was supported by the National Natural Science Foundation of China (Grant No.41902026) and Jiangsu Provincial Marine Science and Technology Innovation Special Project (Grant No. JSZRHYKJ202206 and JSZRHYKJ202001).

Acknowledgments

We thank TC.H and DG.W for assistance of manuscript revision and idea discussion.

Conflict of interest

The author(s) declared that this work was conducted in the absence of any commercial or financial relationships that could be construed as a potential conflict of interest.

Generative AI statement

The author(s) declared that generative AI was not used in the creation of this manuscript.

Any alternative text (alt text) provided alongside figures in this article has been generated by Frontiers with the support of artificial intelligence and reasonable efforts have been made to ensure accuracy, including review by the authors wherever possible. If you identify any issues, please contact us.

Publisher's note

All claims expressed in this article are solely those of the authors and do not necessarily represent those of their affiliated organizations, or those of the publisher, the editors and the reviewers. Any product that may be evaluated in this article, or claim that may be made by its manufacturer, is not guaranteed or endorsed by the publisher.

References

Alexander, C., DeMaster, D., and Nittrouer, C. A. (1991). Sediment accumulation in a modern epicontinental-shelf setting: the Yellow Sea. *Mar. Geol.* 98, 51–72. doi: 10.1016/0025-3227(91)90035-3

Boyko, V., Blonder, B., and Kamyshny, A. (2019). Sources and transformations of iron in the sediments of the Gulf of Aqaba (Red Sea). *Mar. Chem.* 216, 103691. doi: 10.1016/j.marchem.2019.103691

Canfield, D. E. (1997). The geochemistry of river particulates from the continental USA: Major elements. *Geochim. Cosmochim. Acta* 61, 3349–3365. doi: 10.1016/s0016-7037(97)00172-5

Fan, R., Zhao, Y., Chen, Y., Ouyang, L., Jiang, W., Li, N., et al. (2024). Effects of Spartina alterniflora invasion on macrobenthic communities in the Rudong tidal flat. *Fishery Inf. Strategy* 39, 271–281. doi: 10.13233/j.cnki.fishis.2024.04.005

Fen, H., Zhang, T., Zhao, H., Zhu, Z., Geng, Q., Yang, W., et al. (2024a). Research progress on the impact of Spartina alterniflora control on coastal wetland ecosystems. *Wetland Sci. Manage.* 20, 2–6. doi: 10.3969/j.issn.1673-3290.2024.05.01

Feng, Y., Hao, L., Hu, Y., Chu, H., Li, J., Yuan, J., et al. (2024b). Grain size distribution characteristics and transport trends of sediments in the Caofeidian sea area of Bohai Bay. *Mar. Geology Front.* 40, 57–69. doi: 10.16028/j.1009-2722.2024.089

Folk, R. L. (1971). Longitudinal dunes of the northwestern edge of the Simpson Desert, Northern Territory, Australia, 1. Geomorphology and grain size relationships. *Sedimentology* 16, 5–54. doi: 10.1111/j.1365-3091.1971.tb00217.x

Gao, J., Ou, W., Yang, G., Wang, X., and Xu, Q. (2005). Distribution characteristics of sediments in different ecological zones of the North Jiangsu tidal flat. *Donghai Mar. Science/Donghai Haiyang* 23, 40–47.

Gao, S. (2017). A modern process perspective for sedimentary record analysis. *Acta Sedimentologica Sinica/Chenji Xuebao* 35, 918–925. doi: 10.14027/j.cnki.cjxb.2017.05.005

Gebert, J., and Zander, F. (2024). Aerobic and anaerobic mineralisation of sediment organic matter in the tidal River Elbe. *J. Soils Sediments* 24, 2874–2886. doi: 10.1007/s11368-024-03799-6

Gilleaudeau, G. J., and Kah, L. C. (2015). Heterogeneous redox conditions and a shallow chemocline in the Mesoproterozoic ocean: Evidence from carbon–sulfur–iron relationships. *Precambrian Res.* 257, 94–108. doi: 10.1016/j.precamres.2014.11.030

Han, Y., Ren, J., Li, Q., Sun, W., Li, T., and Zhu, M. (2023). Iron geochemistry in surface sediments of the subtropical northern South China Sea and a comparison with the temperate East China Sea. *J. Mar. Syst.* 240, 103878. doi: 10.1016/j.jmarsys.2023.103878

He, J., Fu, C., Su, L., Zhang, G., and Wan, K. (2021). Status and causes of coastal erosion and siltation in Yancheng, Jiangsu Province. *J. Geol.* 45, 189–196. doi: 10.3969/j.issn.1674-3636.2021.02.010

He, P., Wu, H., Cao, B., Gao, Q., and Xu, C. (2020). Analysis of water level variation characteristics in Jiangsu coastal waters. *Mar. Forecasts* 37, 54–59. doi: 10.11737/j.issn.1003-0239.2020.02.007

Hu, L., Ji, Y., Zhao, B., Liu, X., Du, J., Liang, Y., et al. (2023). Iron's impact on organic carbon preservation in marine sediments and its significance for carbon sinks. *Sci. China Earth Sci.* 53, 1967–1981. doi: 10.1007/s11430-023-1139-9

Huang, W., Guo, X., Zhao, J., Li, D., Hu, J., Zhang, H., et al. (2023). Low content of highly reactive iron in sediments from Prydz Bay and the adjacent Southern Ocean: Controlling factors and implications for sedimentary organic carbon preservation. *Front. Mar. Sci.* 10, 1142061. doi: 10.3389/fmars.2023.1142061

Li, C., Planavsky, N. J., Shi, W., Zhang, Z., Zhou, C., Cheng, M., et al. (2015). Marine redox conditions in the middle Proterozoic ocean and isotopic constraints on authigenic carbonate formation: Insights from the Chuanlinggou Formation, Yanshan Basin, North China. *Geochim. Cosmochim. Acta* 150, 90–105. doi: 10.1016/j.gca.2014.12.005

Li, H., Yin, Y., Shi, Y., He, H. C., and Liu, X. (2010). Micro-geomorphology and modern sedimentation rates of the Rudong tidal flat, Jiangsu Province. *J. Palaeogeogr.* 12, 329–338.

Li, Y., Zhang, H., Tu, C., Fu, C., Xue, Y., and Luo, Y. (2016). Sources and fate of organic carbon and nitrogen from land to ocean: Identified by coupling stable isotopes with C/N ratio. *Estuar. Coast. Shelf Sci.* 181, 114–122. doi: 10.1016/j.ecss.2016.08.024

Ma, W. W., Zhu, M. X., Yang, G. P., and Li, T. (2018). Iron geochemistry and organic carbon preservation by iron (oxyhydr) oxides in surface sediments of the East China Sea and the south Yellow Sea. *J. Mar. Syst.* 178, 62–74. doi: 10.1016/j.jmarsys.2017.10.009

Martin, J. M., and Meybeck, M. (1979). Elemental mass-balance of material carried by major world rivers. *Mar. Chem.* 7, 173–206. doi: 10.1016/0304-4203(79)90039-2

Milliman, J. D., Yun-Shan, Q., Mei-e, R., and Saito, Y. (1987). Man's influence on the erosion and transport of sediment by Asian rivers: the Yellow River (Huanghe) example. *J. Geol.* 95, 751–762. doi: 10.1086/629175

Morton, B., and Blackmore, G. (2001). South China sea. *Mar. pollut. Bull.* 42, 1236–1263. doi: 10.1016/s0025-326x(01)00240-5

Nicholls, R. J., and Cazenave, A. (2010). Sea-level rise and its impact on coastal zones. *Science* 328, 1517–1520. doi: 10.1126/science.1185782

Pasquier, V., Fike, D. A., Revillon, S., et al. (2022). A global reassessment of the controls on iron speciation in modern sediments and sedimentary rocks: A dominant role for diagenesis[J]. *Geochimica et Cosmochimica Acta* 335, 211–230. doi: 10.1016/j.gca.2022.08.037

Peng, J., Chen, H., and Ma, S. (2014). Magnetic characteristics and sedimentary environment analysis of tidal flat sediments in the Yellow River Delta. *Scientia Geographica Sinica/Dili Kexue* 34, 1262–1269. doi: 10.1007/978-981-97-7259-9_16

Poulton, S. W., and Canfield, D. E. (2005). Development of a sequential extraction procedure for iron: implications for iron partitioning in continentally derived particulates. *Chem. Geol.* 214, 209–221. doi: 10.1016/j.chemgeo.2004.09.003

Poulton, S., and Raiswell, R. (2002). The low-temperature geochemical cycle of iron: from continental fluxes to marine sediment deposition. *Am. J. Sci.* 302, 774–805. doi: 10.2475/ajs.302.9.774

Poulton, S. W., and Raiswell, R. (2005). Chemical and physical characteristics of iron oxides in riverine and glacial meltwater sediments. *Chem. Geol.* 218, 203–221. doi: 10.1016/j.chemgeo.2005.01.007

Qian, Q., Zhong, S., Li, T., and Wen, D. (2002). Geochemical characteristics and petrogenesis of the Badaling basic rocks and high Ba-Sr granites: Comparison of Mesozoic magmatic rocks in the North China Craton and the Dabie-Sulu Orogen. *Acta Petrologica Sin.* 18, 275–292.

Raiswell, R., and Canfield, D. E. (1998). Sources of iron for pyrite formation in marine sediments. *Am. J. Sci.* 298, 219–245. doi: 10.2475/ajs.298.3.219

Raiswell, R., and Canfield, D. E. (2012). The iron biogeochemical cycle past and present. *Geochem. Perspect.* 1, 1–220. doi: 10.7185/geochempersp.1.1

Roberts, W., Le Hir, P., and Whitehouse, R. (2000). Investigation using simple mathematical models of the effect of tidal currents and waves on the profile shape of intertidal mudflats. *Cont. Shelf Res.* 20, 1079–1097. doi: 10.1016/s0278-4343(00)00013-3

Su, G., Chen, S., Xu, C., Wu, W., Liu, Z., and Fan, Y. (2018). Quantitative inversion of tidal flat elevation in the Yellow River Estuary based on GF-1 images. *Mar. Geology Front.* 34, 1–9. doi: 10.16028/j.1009-2722.2018.11001

Vosteen, P., Spiegel, T., Gledhill, M., Frank, M., Zabel, M., and Scholz, F. (2022). The fate of sedimentary reactive iron at the land-ocean interface: A case study from the Amazon shelf. *Geochem. Geophys. Geosyst.* 23, e2022GC010543. doi: 10.1029/2022gc010543

Wang, A., Gao, S., Jia, J., and Pan, S. (2005). Modern sedimentation rates of the Wanggang salt marshes, Jiangsu. *Acta Geographica Sinica/Dili Xuebao* 60, 61–70. doi: 10.1360/gs050208

Wang, Q., Wang, X., Li, X., Wang, X., and Zhan, C. (2017). Characteristics of surface sediment grain-size and the coarsening phenomenon of the intertidal flat in the abandoned Yellow River Delta. *Quaternary Sci.* 37, 353–367. doi: 10.1007/978-981-97-7259-9_16

Wei, S., Meng, N., Wei, Q., and Zhuang, G. (2024). Comparative study on the characteristics of reactive iron and manganese in sediments and its significance for organic carbon mineralization: A case study of the Yangtze River Estuary, the muddy area of the Central Yellow Sea Shelf, and the Yellow River Estuary. *Adv. Mar. Sci.* 42, 643–662. doi: 10.12362/j.issn.1671-6647.20230823002

Xia, F., Zhang, Y., and Liu, D. (2021). Rethinking on shallow sedimentary sequence and its evolution of the Xiyang tidal channel in the Radial Sand Ridge Field, South Yellow Sea. 41 (04), 13–26. doi: 10.16562/j.cnki.0256-1492.2021033101

Xiang, L., Wang, Y., Jiang, C., Liu, Q., and Li, W. (2024). Distribution, sources, and pollution assessment of heavy metals in surface sediments of intertidal flats in central Jiangsu. *Mar. Geology Front.* 40, 42–52. doi: 10.16028/j.1009-2722.2023.222

Xie, X., Sun, X., Wu, T., Jiang, G., Pu, L., and Xiang, Q. (2020). Effects of Spartina alterniflora invasion on coastal wetland ecosystems: A review. *Chin. J. Appl. Ecol.* 31, 2119–2128. doi: 10.13287/j.1001-9332.202006.032

Xu, F., Li, A., Wan, S., Liu, J., Xu, Z., Xiao, S., et al. (2009). Constraints of mineralogical composition on grain size and geochemical components of terrigenous matter in the inner shelf of the East China Sea. *Earth Sci.* 34, 613–622.

Xue, C., Zhou, Y., and Zhu, X. (2004). The course of the Yellow River and the Yellow River Delta from the end of the Late Pleistocene to the 7th century BC. *Acta Oceanologica Sinica/Haiyang Xuebao* 26, 48–61.

Yang, D., Chen, W., Huang, W., Zhang, H., Han, Z., Lu, B., et al. (2024). Spatial and historical patterns of sedimentary organic matter sources and environmental changes in the Ross Sea, Antarctic: implication from bulk and n-alkane proxies. *Front. Mar. Sci.* 11, 1474189. doi: 10.3389/fmars.2024.1474189

Zhang, L., and Chen, S. L. (2014). Evolution pattern of the Abandoned Yellow River Delta in northern Jiangsu in the past 800 years. *Oceanologia Limnologia Sin.* 45, 626–636.doi: 10.11693/hyhz20130228002

Zhang, H., Sun, T., Zhou, Z., Cao, H., Qiu, J., and Huang, X. (2022). Increased river flow enhances the resilience of spatially patterned mudflats to erosion. *Water Res.* 220, 118660. doi: 10.1016/j.watres.2022.118660

Zhang, Y., Zhang, Z., Ren, H., Gao, L., and Ding, H. (2018). Sources and quantitative estimation of tidal flat sediments at Qidongzui, Yangtze River Estuary during the last century. *Acta Geographica Sinica/Dili Xuebao* 73, 2105–2116. doi: 10.11821/dlxb201811005

Zhao, Y., Xu, M., Liu, Q., Shu, Q., and Wang, P. (2021). Centennial-scale environmental changes recorded by elemental geochemistry of sediments in the Radial Sand Ridges, Northern Jiangsu. *Acta Oceanologica Sinica/Haiyang Xuebao* 43, 66–80. doi: 10.12284/hyxb2021098

Zhou, J., Zhang, L., Zhang, J., Gan, S., Lu, Z., Qin, G., et al. (2024). Blue carbon storage of tidal flats and salt marshes: A comparative assessment in two Chinese coastal areas. *Palaeogeogr. Palaeoclimatol. Palaeoecol.* 655, 112509. doi: 10.1016/j.palaeo.2024.112509

Zhu, X. (2008). *Sedimentary Petrology* (Beijing: Petroleum Industry Press).